

# On the Growth and Collapse of Mixed Regions in Stratified Fluids

K. G. WILLIAMS

*Physical Oceanography Branch  
Ocean Sciences Division*

September 25, 1973



**NAVAL RESEARCH LABORATORY**  
Washington, D.C.

**PREVIOUS REPORT IN THIS SERIES**

"Internal Wave Generation Caused by the Growth and Collapse of a Mixed Region," by J. M. Bergin, NRL Report 7568, June 29, 1973.

## CONTENTS

Abstract .....	ii
Problem Status .....	ii
Authorization .....	ii
PRÉCIS .....	iii
INTRODUCTION .....	1
EXPERIMENTAL .....	1
RESULTS AND DISCUSSION .....	3
Temperature Profiles .....	3
Time Histories .....	5
Studies of Wave Fields, Excitation Time Varied .....	10
TIME HISTORY OF $\Delta H$ .....	18
EFFECT OF GENERATOR ROTATIONAL VELOCITY .....	25
WAVE PROPAGATION .....	25
DISCUSSION .....	27
Background and Definitions .....	27
Interpretation of Experimental Results .....	29
CONCLUSION .....	31
RECOMMENDATION .....	31
REFERENCES .....	31

## ABSTRACT

Experimental observations were made of the development of a mechanically generated, mixed region in the interior of a density-stratified fluid. The results showed that internal waves were initiated in the exterior unmixed fluid before the mixed region reached its maximum vertical extent and began to collapse.

## PROBLEM STATUS

This is a final report on one phase of a continuing problem.

## AUTHORIZATION

NRL Problem G01-06  
Project W-11-125-703

Manuscript submitted March 23, 1973.

## PRECIS

Recent publications have discussed the collapse of mixed regions in the interior of density-stratified fluids, with formation of internal waves. The mathematical description of this process requires a source model, or forcing function, which is simple enough to allow solutions but does not do violence to the basic physics of the problem. These dual requirements are not easily met where the mixed interior region is generated by a localized and transient source of turbulence, an extremely complex and poorly understood process, especially in stratified fluids. Therefore, current source models contain many simplifying assumptions which cannot be fully justified. The work reported here is an experimental "first look" at some basic properties of growth and subsequent collapse of a mixed region, undertaken to clarify the interdependence of separately definable dynamical and buoyant contributions to the wave generation process.

The development of internal waves by local mixing in the interior of a density-stratified fluid was studied experimentally. In the vicinity of a turbulent region generated in thermally stratified water by an axisymmetric mixer, temperature measurements were made in order to follow vertical water displacements in the time frame of 1/30th to 10 Väisälä-Brunt periods in the ambient water.

Preliminary studies showed that standard ensemble averaging techniques could be used for statistically describing certain average properties of the wake. However, the utility of such averaging was brought into question on finding that internal waves apparently were initiated in the exterior fluid at the start of the mixing cycle, and were well developed before the mixed region attained its maximum vertical expansion and began to collapse. Thus, the averaging tended to destroy relevant cyclic information about the early dynamic features of the process and thereby obscured the essential continuity of the overall excitation.

To explore this new concept, a series of measurements was initiated in which the excitation time of the mixer was varied from 1 to 33 s to cover a range of 0.03 to 1.0 Väisälä periods. Temperature vs time measurements were made at a point slightly above and outside the region where primary turbulent mixing occurred. The temperature response was immediate (i.e., less than a second) to agitation of the mixer and was consistently in a direction which indicated an initial downward movement of the local isotherm. This immediate response developed smoothly into a wavelike disturbance with characteristic periods like the local Väisälä period. At very short mixer excitation times, the waveform was nearly sinusoidal, but with increasing excitation time, progressively more complex waveforms appeared. The phasing of various cyclic components appeared to progress through alternate regimes of reinforcement and cancellation as the ratio of the excitation time to the Väisälä period was progressively increased. However, the amplitude of the cyclic components was found to be a nearly linear function of the total excitation time and/or the surface velocity of the mixer.

In addition to cyclic components at the Väisälä period, a net average displacement of the isotherm from its original position which persisted for several Väisälä periods was

observed in the data. This displacement increased from zero to a maximum value at about one Väisälä period and decayed slowly with further increase of time. The mean value, averaged over the observation period, was a linear function of the excitation time and/or surface velocity of the mixer.

These findings led to a hypothesized conceptual model which first provides for the immediate generation of waves by an impulsive process. The potential energy contained in the buoyancy deficit within the mixed region is then retrieved progressively. The specific impulse mechanism is tentatively being attributed to local variations in axial or tangential transport of momentum by viscous processes, with the generation of unbalanced velocity gradients having vertical components which couple into internal waves. Even though oppositely directed components may ultimately cancel, their initial impact on the resonant water system may be deterministic.

Because of the conceptual importance of the immediate initiation of the wave field, several independent tests were made to establish the point. The principal evidence lies in the immediate response of a thermistor above the wake axis and outside the region of primary mixing: For two series of about 15 runs each, the initial responses were essentially identical, though the total mixing time for specific runs varied from 1 to 30 s. This was supported by measurements of the arrival time of the first internal wave crest at various distances from the wake axis; the apparent propagation velocity was proportional to the square root of the displacement without any zero correction as would be required if onset of the wave field were not immediate. A third test involved an investigation of the cumulative displacement of the steady component of flow above the wake axis with time. This required a complicated analysis employing ensemble averaging over a range of mixing times to eliminate effects of cyclic components, together with two normalizations to correct for the density gradient and source strength. The results are therefore accepted only tentatively, but they seem to support the other cited evidence and suggest that flow driven by gravitational forces is present within the mixed region from the first moment of initiation of the mixing process.

Extension of this work is recommended, with emphasis on other experiments which may assist conceptualization and development of a suitable forcing function to accommodate the apparently continuous nature of the coupling of the system to the external fluid.

# ON THE GROWTH AND COLLAPSE OF MIXED REGIONS IN STRATIFIED FLUIDS

## INTRODUCTION

Numerical techniques for performing complex hydrodynamic calculations, such as the particle and cell methods of Harlow (1), have been adapted by Wessel (2) to calculate internal wave fields attributed to the gravitational collapse of mixed waters in turbulent wakes. The procedure required a specified initial condition which represents the cross section of the fully expanded wake. The wake model, conceptually, is set into the density gradient of the calculation plane as a bounded area in which the water is mixed, i.e. the density gradient  $d\rho/dz$  is either zero or somewhat less than the ambient gradient. The computation begins at  $t = 0$ , with the release of constraints on this initially strained condition. The resulting fluid motions are followed, yielding information on the time history of the wave field and its derivative parameters.

This calculation, or an equivalent, is of great importance for describing properties of the internal wave field. However, a careful study of the source conditions used for the calculation is warranted, to avoid serious interpretive errors. To this end, laboratory observations were made in the vicinity of a simulated wake source to measure the degree of mixing and other local characteristics of the growth stage of the wake. The results suggested a new way of conceptualizing the wave generation process which may possibly be of some use for the refinement of computational procedures.

## EXPERIMENTAL

Observations were made in an apparatus basically similar to one used previously by Wu (3) and by van de Watering (4). A Plexiglas tank 175 cm long, 76 cm wide, and 26 cm deep (Fig. 1), was filled from the bottom with water of programmed temperature to produce a stable density gradient. A turbulence generator, which could be rotated back and forth to produce a mixed region, extended across the width of the tank. Two different mixers were used. The first consisted of a 40-mm-diam cylinder of 1/4-in.-mesh hardware cloth, supported on a spiral arrangement of flat paddles (13 by 15 mm) soldered to a 1/4-in.-diam brass rod at angular increments of  $120^\circ$ . The second generator consisted of a 3/8-in.-diam rod, wound with an open spiral of wire about 3/16 in. in diameter. Both generators were rotated by a cam-driven nylon belt, at speeds controlled by an electric motor.

Fluid flows were sometimes followed visually by introducing vertical dye strands or by injecting neutrally buoyant dyes into the core of the mixer. Quantitative temperature measurements were made using a thermistor having a time constant of 0.2 s which could be positioned anywhere in the tank or driven vertically at uniform rates of 27.2, 13.6, 6.8, 3.4, 1.7, or 0.85 cm/min. The thermistor output was presented to the y-axis of an x-y plotter with full-scale (18 cm) sensitivities from less than  $1^\circ\text{C}$  to more than  $150^\circ\text{C}$ .

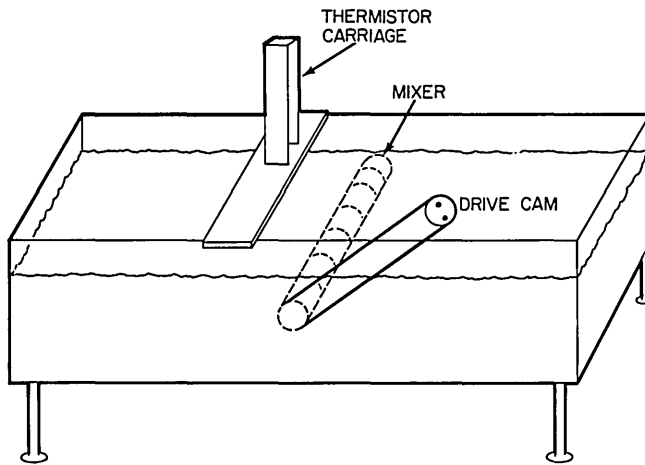


Fig. 1 — The experimental tank was of Plexiglas, 69 in. long, 30 in. wide and 10 in. deep. The cylindrical turbulence generator (mixer) extended across the width of the tank, and was oscillated back and forth by a motor drive. The thermistor carriage could be fixed at any point in the tank or driven vertically at predetermined rates.

Either time or vertical displacement of the thermistor could be presented to the  $x$ -axis. Time scales covering 0.2 to 20 s/cm and dimensional magnifications of 1/5 to 100 times the actual vertical thermistor displacement were available.

In operation, the tank was half filled with water a few degrees cooler than the local air temperature. A second, more dense layer, perhaps  $10^{\circ}\text{C}$  cooler, was then introduced beneath the first through a diffusing screen placed over the bottom fill pipe. After filling, 30 to 60 min was allowed so that movements generated by filling would damp out, and a vertical temperature profile was taken. The thermistor was then repositioned,\* the turbulence generator was actuated, and the desired measurements were made. New experiments were initiated after the disturbance had damped sufficiently. The temperature of the upper layer usually remained constant throughout the day's operation; the lower layer, warmed by conduction through the tank bottom and gradually mixed with the upper layer water, became progressively warmer. The average Brunt-Väisälä period† typically increased from values like 25 s in the early morning to 40 or 50 s in the late afternoon. (The time variance of the temperature gradient required frequent profiling to maintain the desired knowledge of the test condition.)

\*All measurements were made with the thermistor moving downward to minimize temperature anomalies known to result from viscous flow along the thermistor.

†Calculated from  $T_{BV} = 2\pi [(\rho \Delta Z)/(G \Delta \rho)]^{1/2}$ , where  $\Delta Z$  was taken as 0.75 ft,  $G = 32.2 \text{ ft/s}^2$ ,  $\rho = 1.000$ , and  $\Delta \rho$  is the density difference, from published tables of water density vs temperature.

Two types of measurements were made. First, sequential plots of temperature vs depth were taken through vertical sections of the mixed region to display changes introduced into the profile by the mixing. In brief, a profile would be taken, the generator actuated, and subsequent profiles made. The resulting records, while displaying the depth variation of temperature, also contained time variance information. To avoid this ambiguity, time histories of the temperature were made with the thermistor fixed in a pre-selected location. Coverage of the wake region was obtained by repeating runs with the thermistor at different locations.

## RESULTS AND DISCUSSION

Approximately 100 test runs were made, involving variations of thermistor position, density gradient, and source strength.

### Temperature Profiles

Vertical temperature profiles made shortly before and after generator excitation, and at some later time, yielded series of plots similar to those shown in Fig. 2. The results were influenced by the time delay  $t_d$  between excitation and observation, the thermistor descent rate, and the lateral displacement of the measurement point from the generator axis. Measurements made where  $t_d > 120$  s displayed only wavelike perturbations of the profile (Fig. 2a). The waveform and period of the system response, typically 20 to 60 s, the delay time, and the rate of thermistor travel determined the shape and position of the maximum lateral excursions. This group of measurements was also nearly free of erratic, turbulent-like bursts and seemed to display characteristics of a propagating wave field rather than those of a mixed region.

At shorter delay times of 60 to 120 s, occasional spasmodic irregularities appeared in the record, in addition to the waves, which were taken to be evidence of turbulent mixing, particularly for measurements close to the generator. A typical plot is given in Fig. 2b for a lateral thermistor displacement of 25 mm, and in Fig. 2c for a displacement of 150 mm.

Considerably more variability was observed in the curves taken at yet shorter delay times. This is easily seen in Fig. 2d, where the results of two separate trials made at delay times of 14.8 and 7.8 s are superposed on a single graph. The lateral displacement was 22 mm from the axis and 2 mm from the periphery of the turbulence generator.

To quantize the results of the profile measurements, the vertical displacement of the isotherms from their original position was measured for 25 runs at points corresponding

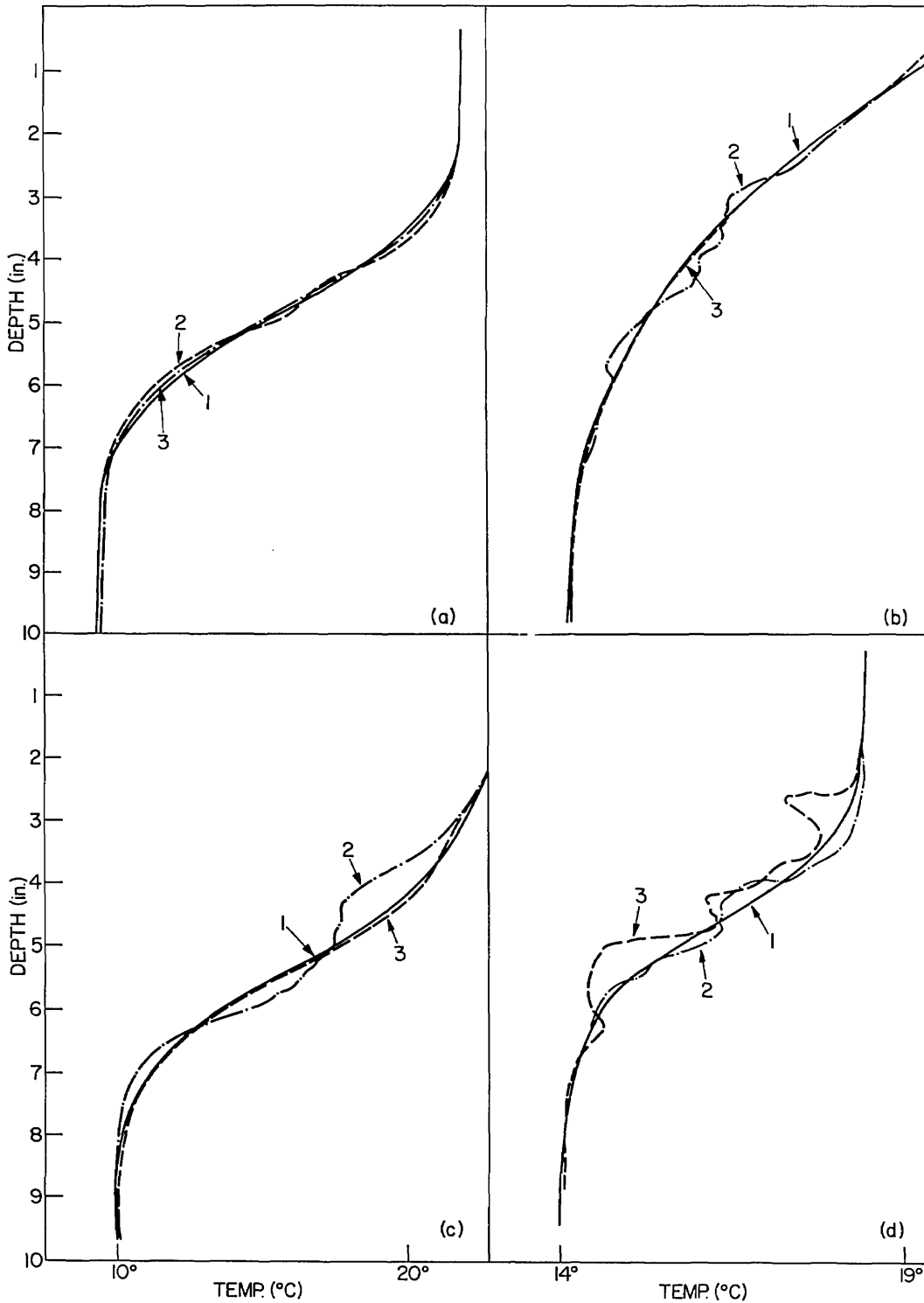


Fig. 2 — Vertical temperature profiles in the tank. In Figs. 2a, b, and c, trace (1) represents the initial condition, (2) was taken after generator excitation, and (3) was taken at a later time. Delay times between mixer excitation and trace (2) were as follows: (a) 2 min, (b) 1 min, and (c) 1 min. In Fig. 2d, trace (1) repeats the initial condition while traces (2) and (3) were taken 7.8 and 14.8 seconds later.

to successive depth increments of 5 mm, from 25 mm below to 25 mm above the generator axis. The displacements were averaged for various delay-time groups and the rms variations determined. The maximum displacement at each depth was also measured, and the average numerical value of the maximum excursions determined. The results are summarized in Table 1. The amplitude of the disturbances clearly falls off with time.

A preliminary estimate of the average extent of mixing was attempted by measuring the isotherm displacement at a number of depths for several runs. Data were taken from 10 recordings at depth increments of 5 mm, from 5 cm below to 5 cm above the mixer axis. The data were folded around the axis and averaged, with the following results.

Vertical Distance from Axis (mm)	Mean Displacement of Isotherm (mm)
0	1.0
5	5.65
10	8.28
15	10.8
20	7.75
25	5.43
30	4.60
35	3.70
40	1.95
45	1.20
50	0.10

The data are plotted in Fig. 3, from which it may be seen that the displacement has resulted in reducing the density gradient in the primary mixing zone by a factor of 0.5. The extent of mixing falls off gradually in the entrainment region outside the mixer.

Because of the unresolvable ambiguities between time and space dependencies which are inherent in this particular measurement, no further efforts were made to study the problem by this technique.

### Time Histories

Typical time history variations are shown in Fig. 4. Measurements made nearest the generator characteristically displayed a brief initial burst of erratic, high-frequency response which modulated into a gentle wavelike undulation. Further away from the source, the

Table 1  
Averaged Summary of Isotherm Displacements

Delay Time Group	Average Isotherm Displacement (mm)	Standard Deviation (mm)	Average of Max. Displacements (mm)	Ratio ( $\frac{\text{Max}}{\text{Av}}$ )
<60	10.9	9.8	31.8	2.92
60-120	4.8	8.0	8.7	1.82
>120	2.2	2.0	5.6	2.54

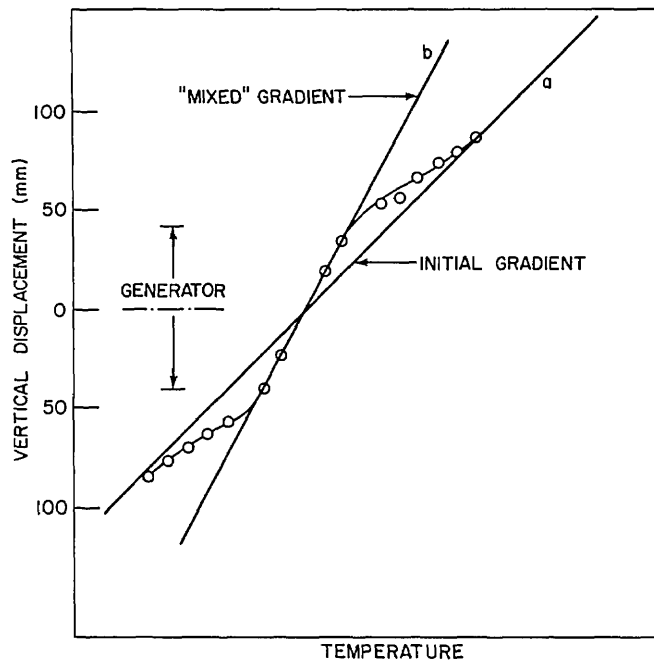


Fig. 3 — Average mixing in wake region. Straight line (a) represents average gradient before mixing; (b) is line with one-half slope of (a) passing through axis of mixed region. Points represent average of several measurements.

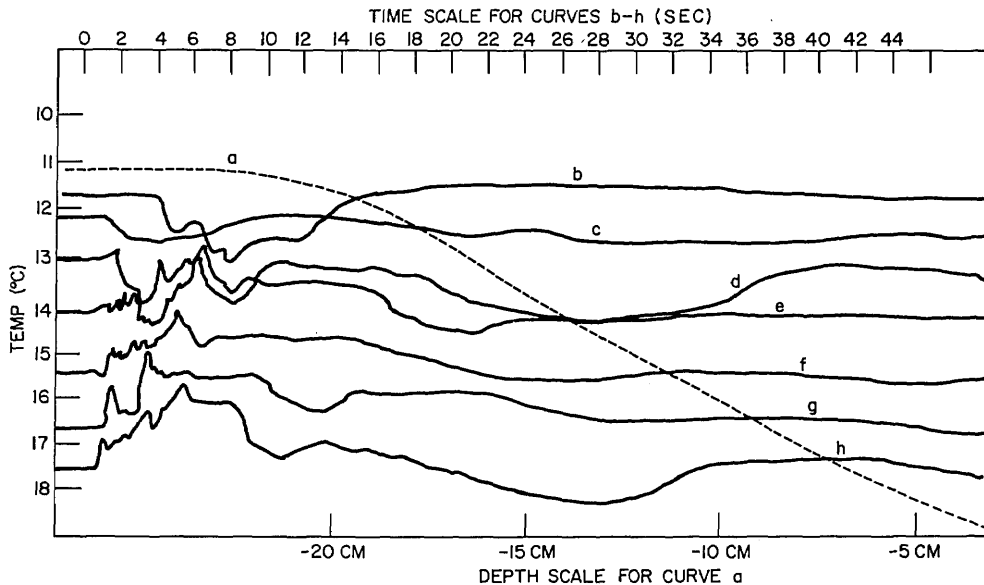


Fig. 4 — Combined temperature profile and time history plot. Curve a shows temperature vs depth in tank before mixing. Plots b-h are time histories made at depths of 19.5, 17.5, 15.5, 13.5, 11.5, 9.5, 7.5, and 5.5 cm, respectively (hardware-cloth mixer).

amplitude of the initial erratic oscillations became less and did not appear at distances of 300 mm, where only wavelike motions are observed. Also, in the vertical dimension little or no erraticity is observed in traces well removed from the generator. These observations agree with visual observations of dye tracers; quite thorough mixing occurred on a small scale near the mixer, and slower movements having dimensional scales like the radius of the mixer moved relatively discrete masses of fluid around in the mixed region. The life-time of individual features was like the period of the oscillations appearing in the traces, i.e., a few seconds.

To investigate the magnitude of typical isotherm displacements, measurements were made from the recordings of 13 runs. Turbulent excursions were first distinguished from wavelike oscillations on the basis of their high-frequency content, and separate measurements were made of the maximum isotherm displacements (crest to trough) associated with turbulence and waves. The results, averaged for various parameters, are summarized in Table 2 and in Fig. 5. The average of the maximum displacement was 8.2 mm. It varied only slightly over a range of lateral displacements up to 7.5 mixer diameters, at all depths except near the surface where wave amplitude approached zero, and over a range of 6 to 1 in the temperature difference between the top and bottom of the tank. Thus wave amplitude was relatively independent of the ambient density gradient for a source of specified dimensions and strength.

Table 2

Lateral Displacement (mm)		Wave Height (mm)	Turbulent Bursts (mm)
22-25		8.45	25.5
50		8.25	16.3
100		9.01	5.1
150		8.00	3.1
300		10.1	0.0
Depth (cm below surface)			
1		5.6	0
3		9.13	0
6		8.3	2
9		12.0	21
12		10.6	17
15		9.0	34
Temperature Difference (°C)	$x^*$ (mm)		
9.0	150	3.2	0
8.1	100	8.0	8.0
7.5	50	8.0	37.5
4.8	22	8.2	32
3.7	50	8.3	11
3.5	50	8.9	43
3.1	22	9.3	43.5
2.7	100	6.9	14
2.7	100	12.8	16
2.2	22	8.0	50
2.0	100	8.0	14
1.9	150	8.0	19
1.6	300	10.0	0

\* $x$  is lateral displacement from mixer axis.

To observe the effect of varying source strength, the standardized mixing conditions which had been adopted for the above observations were changed. These had originally consisted of three full cycles (back and forth) of mixer rotation through  $540^\circ$  at a constant speed setting of maximum. The mean surface velocity and other characteristics of the mixer are indicated below.

Speed Control Setting	Cycles/min	s/Cycle	Mean Surface Velocity (cm/s)
30	24.3	2.46	10.2
50	43.5	1.38	18.21
70	66.7	0.90	27.9
90	90.0	0.66	37.8
Maximum	133.3	0.45	55.8

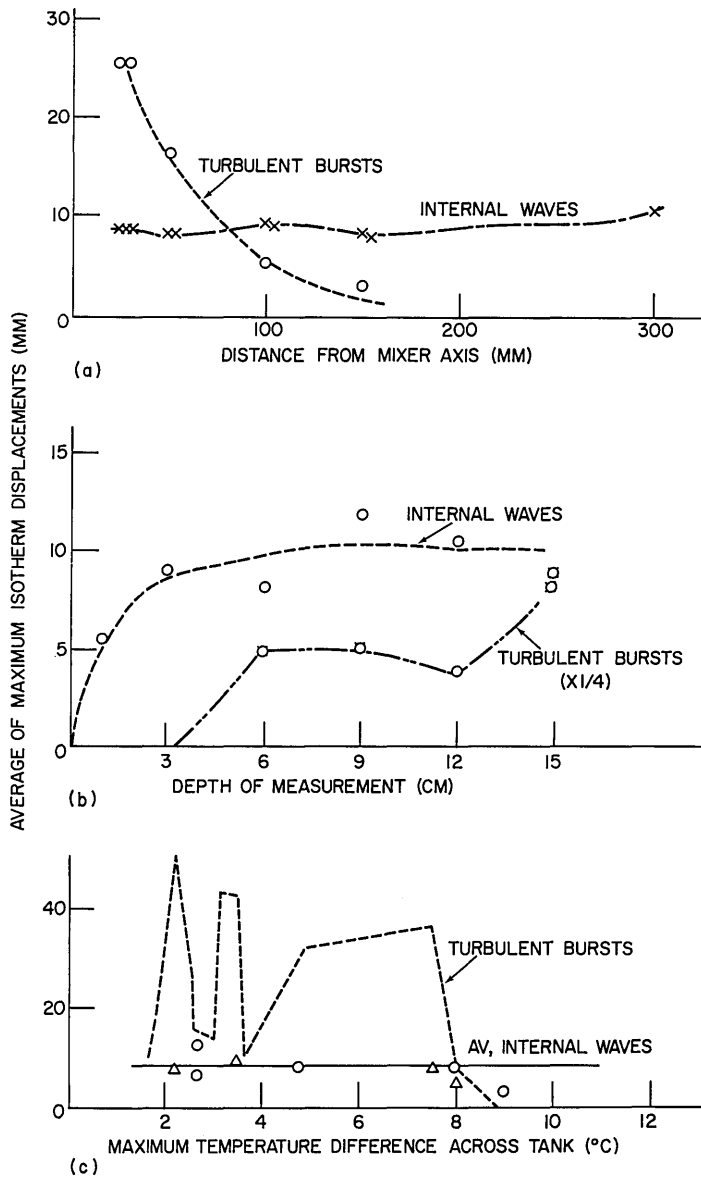


Fig. 5 — Average of maximum isotherm displacements associated with turbulent and wavelike motions for 13 tests: (a) at various horizontal distances from mixer, (b) at various measurement depths, and (c) in various temperature gradients

Table 3  
Average Vertical Isotherm Displacements  
for Various Source Conditions

Run No.	Mixer	Condition Speed	$t_e$ (s)	$U_m$ (cm/s)	$D_m$ (cm)	$U_m^2 t_e$ (cm <sup>2</sup> /s)	Isotherm Displacement (mm)	
							Av	Av Max
3-18-1	3	70	2.7	27.9	76	2101	6.95	14.48
3-18-2	3	50	4.2	18.2	76	1391	6.67	15.0
3-18-3	3	30	7.5	10.2	76	780	7.34	17.3
3-18-4	1	30	2.5	10.2	25	260	3.73	9.3
55	1	70	0.9	27.9	25	700	9.31	19.5
6	5	70	4.5	27.9	126	3503	8.88	20.1

A series of six runs was made, taking 48-s time histories of temperature at 3.4, 7.4, 10.4, and 18.4 cm, and at a lateral displacement of 25 mm from the generator axis. The maximum temperature excursions occurring in the next 2 min were also recorded. The source conditions were varied.

The data were reduced by measuring the isotherm displacement, for each trace, at intervals of 2 s. Data from all measurement depths for that particular time were then averaged, and the average of 24 groups of measurements made during the observation period of 48 s was determined. The result is an overall average value of vertical displacement at five locations over a period longer than the local Väisälä period and throughout a depth range equal to 2.5 mixer diameters. This was expected to give an indication of the total energy transferred to the system by the source.

Since it was expected that the effective source strength would be some function of both the speed of rotation and the duration of the excitation period, the displacements were compared with several source characteristics. The source strength was expressed variously as excitation time  $t_e$ , the total distance of travel of the mixer periphery  $D_m$ , the surface velocity of the mixer,  $U = D_m/t_e$ , and the square of surface velocity multiplied by the excitation time,  $U_m^2 t_e$ . The results are summarized in Table 3. The relationships between average displacement and source strength (Fig. 6) did not immediately suggest strong correlations of appreciable significance, and a more detailed study was initiated.

### Studies of Wave Fields, Excitation Time Varied

A sequence of observations at a single point and at a single source velocity was made with progressive increases of mixing time. The smaller spiral mixer (diam = 20 mm) was used for the experiment to deliberately deemphasize impulsive aspects of the mixing process by increasing the angular symmetry to reduce the range of available dimensional scales. This was done to avoid directed vortex pairs which might be shed from the internal paddles of the mesh cylinder. The thermal history was measured at a point 2 cm above and 1.35 cm off the generator axis in the horizontal. The traces are shown in Fig. 7. Several features may be seen on inspection: (a) the waveform was relatively "clean" for the shortest excitation period but became more complex with increasing time of excitation; (b) the traces departed from the zero position immediately after excitation of the mixer and always moved initially to a warmer condition, corresponding to a locally

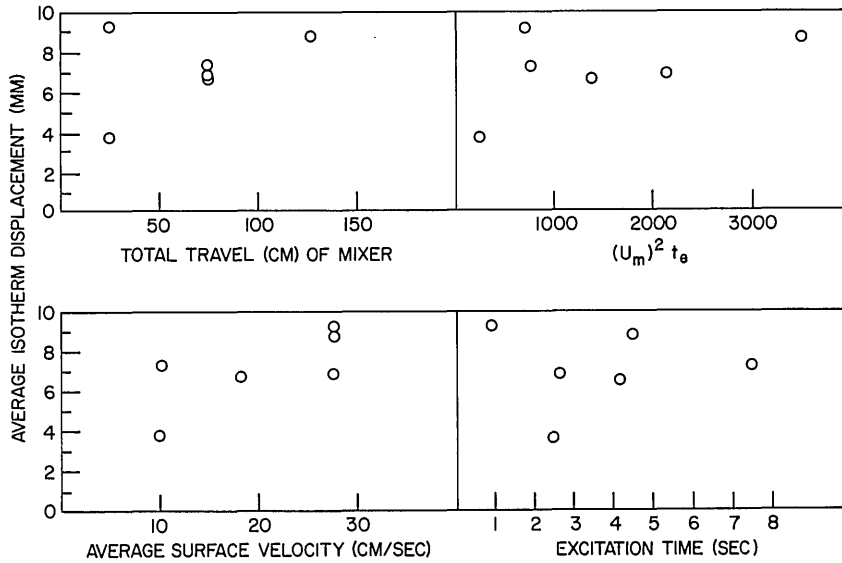


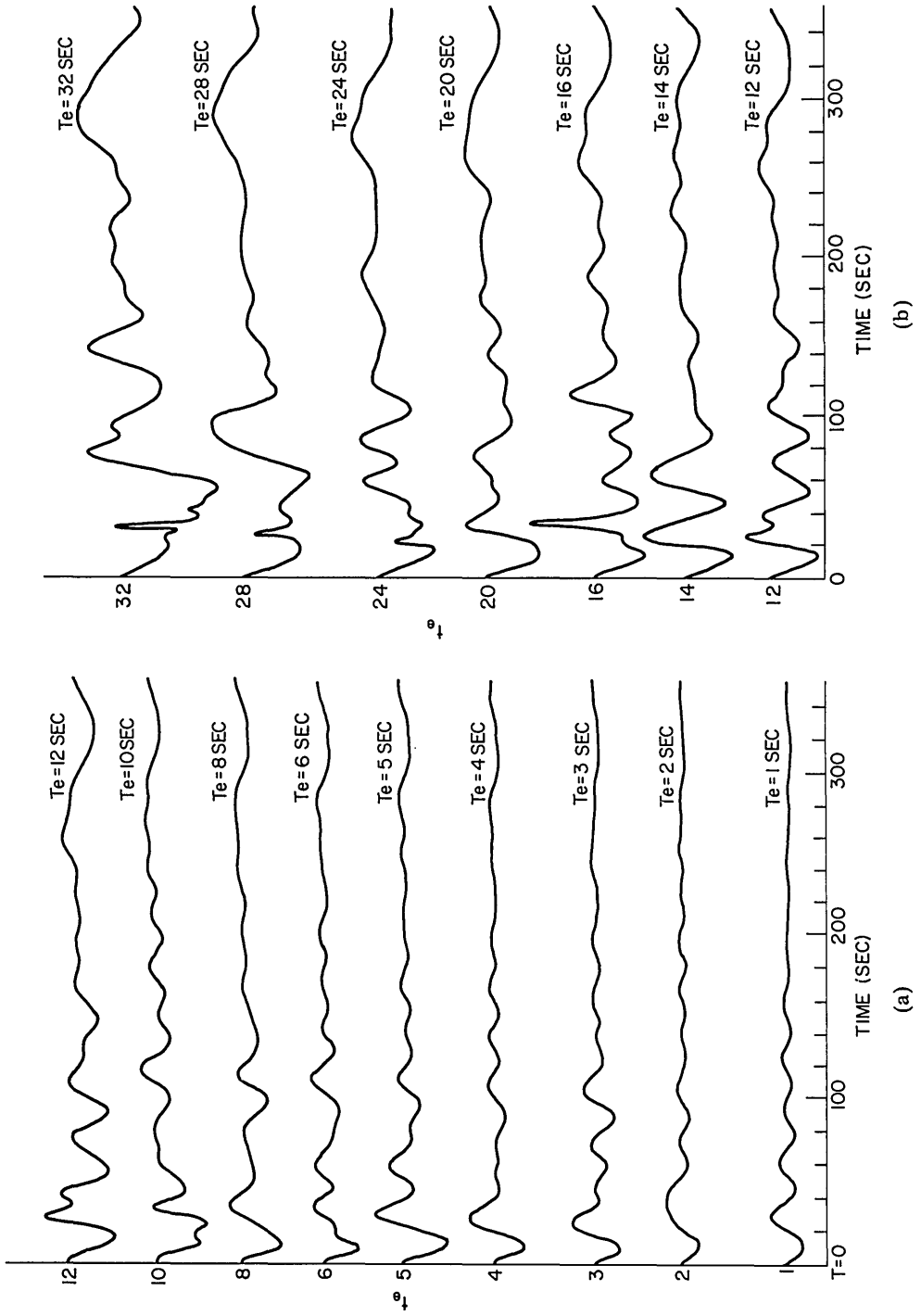
Fig. 6 — Average isotherm displacement for a range of source strengths. Overall average values are plotted against various source strength indicators.

downward movement of water; (c) in addition to the cyclic components of motion having periods like the Brunt-Väisälä period, an asymmetric displacement (nonzero average) was observed, particularly in the later runs, with growth and decay occurring over a time corresponding to several Väisälä periods; (d) no high-frequency components identified as turbulence appear, except possibly at the longest mixing time.

The results were studied quantitatively by measuring the local displacement  $z$  of each individual trace from an arbitrary reference level at equal intervals corresponding to 4 s of real time, over a measurement period of 112 s. For each run, the average level of  $\Sigma z/n$  was determined. The reference level was then subtracted to give the mean displacement from its zero level  $\Delta H$ , and the rms average displacement of fluctuating components  $\sigma$  was determined.\* The results of these measurements are given in Table 4 and in Fig. 8. The magnitudes of both  $\Delta H$  and  $\sigma$  increase with increasing excitation time, but relatively large and sharply peaked departures from a linear relationship appear in both records. Some tendency toward an inverse relationship between deviations in the relative values of  $\Delta H$  and  $\sigma$  was noted: where  $\sigma$  exhibits a local maximum,  $\Delta H$  tends to exhibit a local minimum.

In searching for an explanation of this behavior, a conceptual distinction was made between internal waves and quasi-stationary effects of mixing within the turbulent region. The distinction is based on the ratio of the observation period to the duration of the phenomena: internal waves are considered to have periods like the local Brunt-Väisälä period in the ambient water, whereas quasi-permanent effects are considered to be either noncyclic or heavily damped, or to have a characteristic period at least several times longer than the local Väisälä period in the unmixed ambient water. In this case, the

$$* \sigma = \sqrt{\frac{n(\Sigma z^2) - (\Sigma z)^2}{n^2}}$$



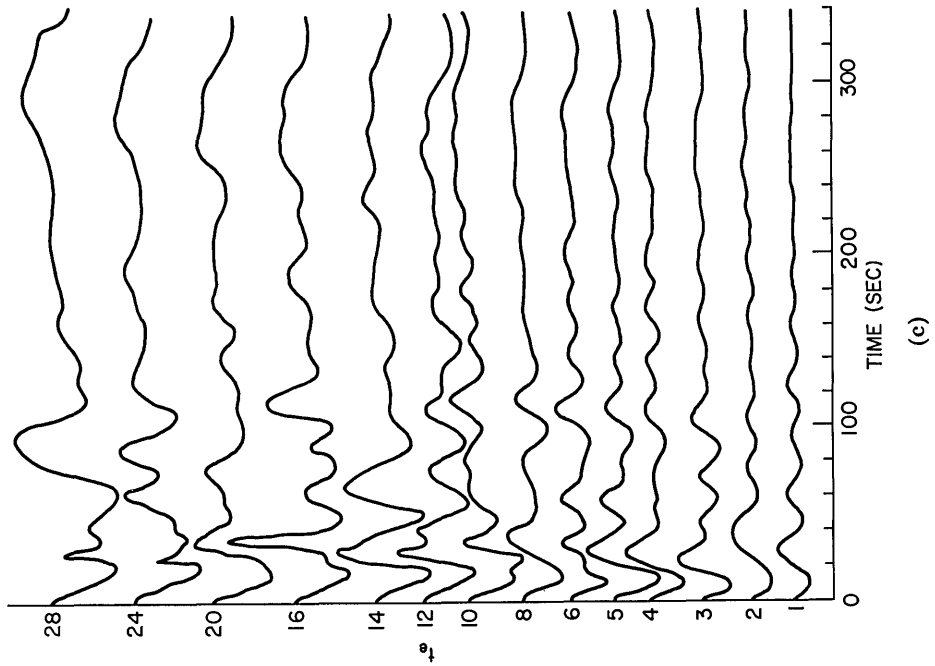


Fig. 7 -- Temperature vs time plots for (a) runs 3-25 (1-12), (b) 3-25 (12-32), and (c) 4-7 (1-28). Measurement point was slightly outside primary mixing zone ( $x = 20$  mm,  $h = 25$  mm). Spiral mixer was used with maximum speed setting. Mixing time is indicated on each plot.

Table 4  
 Statistical Properties of Internal Waves Generated  
 for Various Excitation Times (3-25)

Run	Conversion Factor*	$t_n$ (dimensionless)	$\Delta H$ (mm)	$\sigma$ (mm)	$\sigma/\Delta H$	$(2\sigma + \Delta H)$ (mm)	$\frac{\Delta H}{t_n \dagger \ddagger}$	$\frac{\sigma}{t_n \dagger}$	$\frac{(2\sigma + \Delta H)}{t_n \dagger}$
3-25- 1	0.2269	1.0	0.076	0.469	6.18	1.014	0.076	0.469	1.014
2	0.2323	1.98	0.159	0.646	4.06	1.451	0.080	0.326	0.733
3	0.2377	2.93	0.400	0.892	2.23	2.184	0.136	0.304	0.745
4	0.2430	3.86	0.382	0.895	2.34	2.172	0.099	0.232	0.563
5	0.2484	4.78	0.599	1.223	2.04	3.044	0.125	0.256	0.636
6	0.2538	5.67	0.672	0.920	1.37	2.511	0.118	0.162	0.443
7	0.2592	7.48	0.988	0.965	0.98	2.919	0.132	0.129	0.390
8	0.2645	9.26	1.160	1.377	1.19	3.915	0.125	0.149	0.423
9	0.2700	11.0	1.455	1.472	1.01	4.400	0.132	0.134	0.400
10	0.2753	12.7	0.986	2.123	1.76	5.454	0.078	0.167	0.429
11	0.2807	14.4	1.964	1.880	0.96	5.726	0.136	0.131	0.398
12	0.2860	17.8	1.630	1.656	1.02	4.942	0.091	0.093	0.277
13	0.2915	21.2	2.200	1.776	0.81	5.751	0.103	0.084	0.271
14	0.2968	24.5	2.447	2.016	1.15	8.078	0.100	0.115	0.330
15	0.3022	27.7	3.085	3.351	1.09	9.785	0.113	0.121	0.353
Average	—	—	—	—	—	—	0.1096	0.1914	0.494

\*From millimeter of displacement on chart to millimeter vertical displacement of isotherm.

†Dimensionless time.

‡Millimeter displacement divided by duration of excitation.

observation period of 112 s was long compared to observed wave periods of 30-40 s, but it was somewhat shorter than the estimated restoration time of the collapse process. The magnitude of  $\Delta H$  was considered to be some function of the efficiency of the mixing process, and was believed to represent downward displacement of the local thermocline in response to vertically downward flow components. The measurement point, of course, had been chosen to be outside the region of primary mixing to avoid purely turbulent effects. Sigma ( $\sigma$ ) represents the rms magnitude of cyclic components which are superimposed onto the displacements associated with  $\Delta H$  and is related to the magnitude of internal wave processes.

On the basis of the foregoing distinctions, it was postulated that sensible energy\* transferred to the system by the turbulence generator  $E$  would be proportional to the sum of three components representing (a) the potential energy within the mixed region, (b) the kinetic component of wavelike motions, and (c) the instantaneous potential energy of wavelike displacements. The first of these was assumed to be proportional to  $\Delta H$ ; the other two are related to  $\sigma$ . If an equipartition of energy in the wave field between kinetic and potential modes, a constant density gradient, and geometrically similar conditions are assumed, the wave energy is expected to be proportional to  $2\sigma$ . The total energy was then expected to be proportional to  $(\Delta H + 2\sigma)$ . If it is further assumed that the turbulence generator transfers energy to the water at a uniform rate, the energy input is proportional to excitation time, and  $(\Delta H + 2\sigma)$  should be directly proportional to the excitation time.

Before testing this hypothesis, the raw temperature data were converted to vertical isotherm displacement to eliminate the influence of gradual temperature variations (decreasing with time) which occurred during the sequence of experimental measurements. The necessary conversion factors were computed from the measured slope of the mean temperature-vs-depth profiles taken before and after the series of runs, plus several intermediate calibration measurements made by displacing the thermistor above and below the measurement point. The data used to compute the corrections are shown in Fig. 9. Excitation time was also corrected by multiplying the actual excitation time by the square root of the density gradient ratio for all runs subsequent to the first, thereby expressing time in terms of a characteristic Väisälä period:

$$t_n = t_e \sqrt{\frac{\Delta T}{\Delta T_0}},$$

where

$t_n$  is a normalized time

$t_e$  is the excitation time

$\Delta T$  is the temperature difference across the tank at time  $t$

$\Delta T_0$  is the initial temperature difference.

(It is assumed for this calculation that the density is a linear function of temperature.) The shape of the density-vs-depth plot did not change greatly during any series of runs, so that a more refined correction was not necessary.

\*At temporal scales equal to or greater than the time constant of the thermistor; the energy content of fine scale turbulence was not measured.

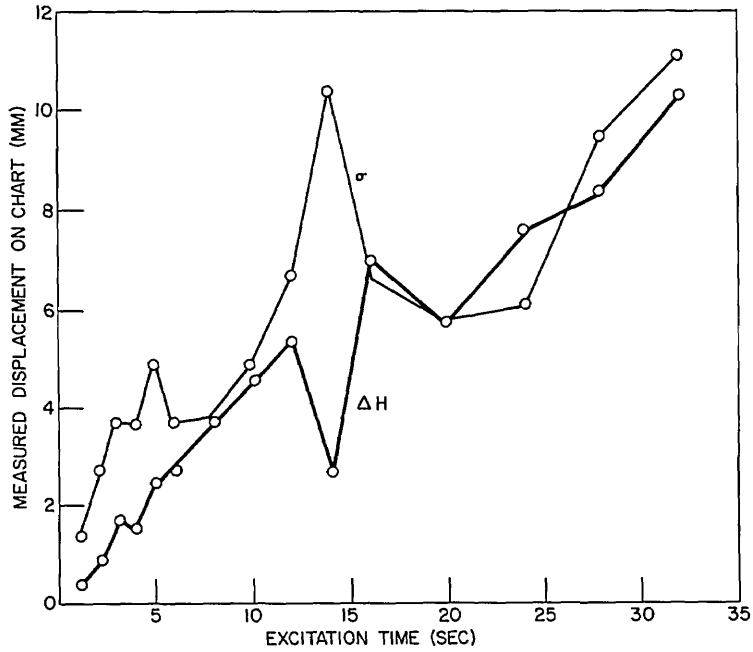


Fig. 8 — Plot of average displacement  $\Delta H$  and rms value of cyclic components  $\sigma$  vs excitation time  $t_e$  for runs 3-25 (1-15)

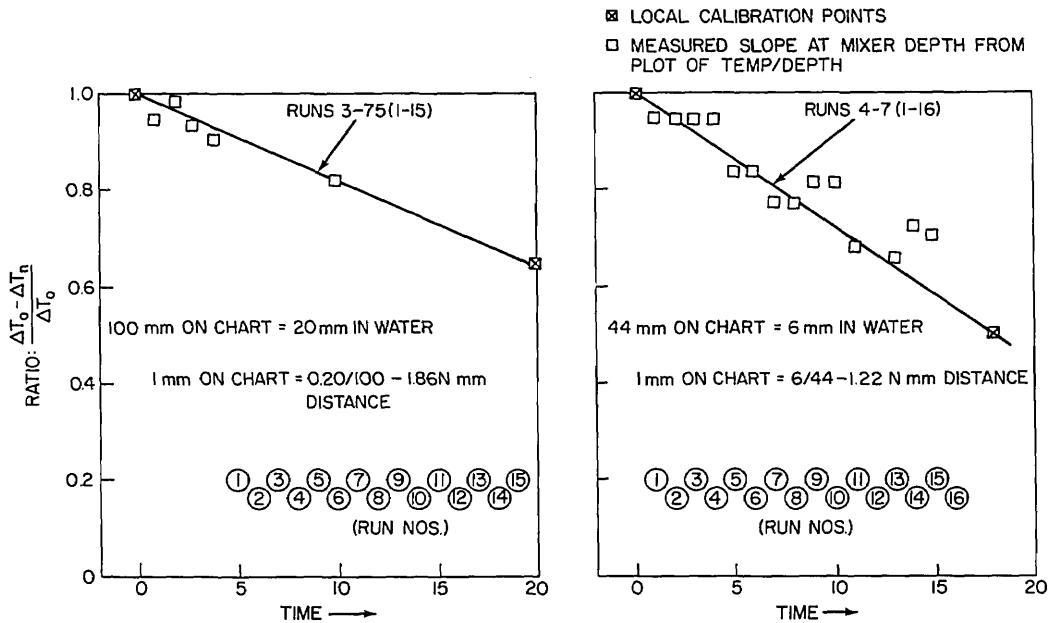


Fig. 9 — Calibration data for conversion of real time to dimensionless time.  $\square$  indicates direct measurement of  $\Delta T/\Delta z$ , by physical displacement of thermistor;  $\boxtimes$  represents determination of  $dT/dz$  from slope of temperature vs depth plot. Data for runs 3-25 (1-15) and 4-7 (1-16) are shown separately.

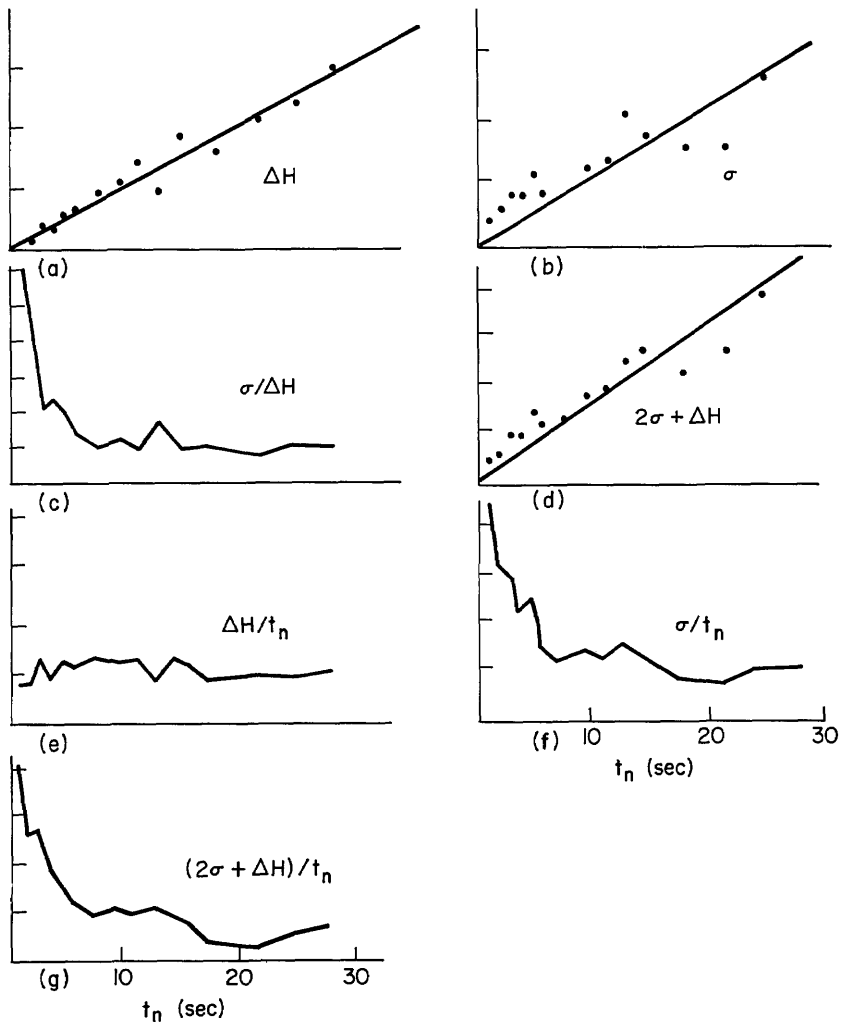


Fig. 10 — Various relationships between average displacement  $\Delta H$ , cyclic components  $\sigma$ , and excitation time  $t_n$ . (a)  $\Delta H$  vs  $t_n$ , (b)  $\sigma$  vs  $t_n$ , (c)  $\sigma/\Delta H$  vs  $t_n$ , (d)  $(2\sigma + \Delta H)$  vs  $t_n$ , (e)  $\Delta H/t_n$  vs  $t_n$ , (f)  $\sigma/t_n$  vs  $t_n$ , and (g)  $(2\sigma + \Delta H)/t_n$  vs  $t_n$  (for runs 3-25 (1-15)).

The results are plotted in Fig. 10a and 10b. The lines drawn through the points are unweighted rms average values. As a first approximation, it appears that both  $\Delta H$  and  $\sigma$  are linear functions of excitation time. However, the apparently systematic deviations of individual data points from the curve can allow other interpretations, and some additional tests were applied. The ratio  $\sigma/\Delta H$  was first calculated for each point and plotted in Fig. 10c. If both  $\sigma$  and  $\Delta H$  were linear functions of excitation time, their ratio would be constant except for random scatter. This did not appear to be the case; the ratio displays a systematic change from a maximum value at short excitation times to a much lower mean value at longer times. In addition, some evidence of periodicity appears. To seek the origin of this systematic deviation, the ratios  $\Delta H/t_n$  and  $\sigma/t_n$  were calculated (columns 7 and 8 of Table 4) and plotted against excitation time (Fig. 10e and 10f). Except for a little scatter of the points,  $\Delta H$  vs  $t_n$  is constant, confirming the approximately linear relationship previously postulated between  $t_n$  and  $\Delta H$ . On the other hand, the plot of  $\sigma/t_n$  is virtually identical with that of Fig. 10c. Thus, short excitation

times are seen to be especially effective for immediate generation of internal waves. The enhanced effectiveness of the generator at short excitation times is reflected also in the curves of 10d and 10g, where the quantities  $(2\sigma + \Delta H)$  and  $(2\sigma + \Delta H)/t_n$  are plotted. The above results suggest very important implications with respect to computational wake models, and a second series of runs was made to see if the results could be duplicated. Small changes in the experiment were introduced to change the ratio of impulse to mixing; the measurement point was moved 5 mm farther away from the generator axis and the speed of rotation of the spiral turbulence generator was reduced from 130 to 60 rpm. A slightly greater density gradient was also used, and more frequent calibrations were made. Otherwise, the experiment duplicated the earlier one. The results are given in Table 5 and are plotted in Fig. 11.

As before,  $\Delta H$ ,  $\sigma$ , and  $(2\sigma + \Delta H)$  increased linearly with excitation time in the first approximation, but the proportionality constant was less and the magnitude of  $\Delta H$  decreased more than the magnitude of  $\sigma$ . These relationships are given numerically below.

<u>Runs 3-25-1 to 15</u>	<u>Runs 4-7-1 to 18</u>
$\Delta H = 0.108 t_n$	$\Delta H = 0.051 t_n$
$\sigma = 0.121 t_n$	$\sigma = 0.090 t_n$
$\sigma/\Delta H = 0.892$	$\sigma/\Delta H = 0.566$

The decreased magnitude of  $\Delta H$  in the second experiment, under conditions less favorable for generation of turbulence, is qualitatively agreeable to the hypothesized identification of  $\Delta H$  with the effects of mixed wake collapse. Also, the decrease in absolute magnitude of  $\sigma$  with decreasing rotational velocity of the mixer is compatible with a postulated impulsive origin of the waves.

Otherwise, the most visible difference between the two experiments is an increased periodicity in the plot relating the magnitude of  $\Delta H$  and  $\sigma$  to the excitation time. This shows up particularly in the ratio  $\sigma/\Delta H$  plotted against  $t_n$  (Fig. 11e). Also, an inverse correlation between peaks in the time plots of  $\Delta H$  and  $\sigma$  can be determined by inspection. Except for this periodicity, the variation of  $\sigma/t_n$  is similar to that for earlier runs. The averaged data for the two sets of runs are given in Fig. 12 to illustrate the general form of the relationships; the peak efficiency of the wave generation at short excitation times decreased rapidly as  $t_n$  was increased up to a quarter of the Väisälä period. Further increases in  $t_n$  had little effect on the ratio.

## TIME HISTORY OF $\Delta H$

The next step in the analysis was an examination of the way in which  $\Delta H$ , the quasi-stationary displacement, actually varied with time. To do this, the cumulative sums of the deviations from zero level at successive time intervals were calculated for each of 10 runs. The results were normalized to set the upper end of each data set at a value of 1.0 and plotted against time (dimensionless) to yield the relationships shown in Fig. 13. Differences between individual curves are quite apparent, but a general trend appeared. This was defined by averaging all values of  $\Delta H$  lying within incremental time groups of 1-s duration. The averages (Table 6) yielded a straight line when plotted on semilog paper (Fig. 14). Two features of this plot are of considerable interest: a straight line can be

Table 5  
 Statistical Properties of Internal Waves Generated for  
 Various Excitation Times (Run 4-7)

Run*	$t_n$ (dimensionless)	$\Delta H$ (mm)	$\sigma$ (mm)	$\sigma/\Delta H$	$2\sigma + \Delta H$ (mm)	$\frac{\Delta H}{t_n \dagger\dagger}$	$\frac{\sigma}{t_n}$	$\frac{2\sigma + \Delta H}{t_n}$
4-7- 1	1.00	0.114	2.174	1.91	0.55	0.144	0.217	0.548
2	1.972	0.1233	0.4103	3.33	0.94	0.063	0.208	0.478
3	2.910	0.1834	0.3971	2.17	0.98	0.063	0.136	0.335
4	3.826	0.2886	0.3583	1.24	1.01	0.075	0.094	0.262
5	4.706	0.5377	0.5315	0.99	1.60	0.114	0.113	0.340
6	5.561	0.3672	0.6916	1.88	1.75	0.066	0.124	0.315
7	6.371	0.3610	0.9183	2.54	2.20	0.057	0.144	0.345
9	7.815	0.4168	0.8813	2.11	2.18	0.053	0.113	0.279
10	9.493	0.5258	0.7234	1.38	1.97	0.055	0.076	0.208
11	10.986	0.7334	0.8330	1.14	2.40	0.067	0.076	0.218
12	12.426	0.5288	1.358	2.57	3.24	0.043	0.109	0.261
13	14.592	0.7468	1.050	1.41	2.85	0.051	0.072	0.195
14	16.676	1.074	1.381	1.29	3.84	0.064	0.003	0.230
15	18.602	0.898	1.239	1.38	3.38	0.048	0.067	0.181
16	20.409	0.998	2.173	2.18	5.34	0.049	0.106	0.262
17	22.143	1.053	2.148	2.04	5.35	0.048	0.097	0.242
18	23.674	2.413	2.352	0.96	7.06	0.102	0.098	0.298

\*Data for Run 4-7-8 were taken at an incorrect depth and were omitted from the table.

†Dimensionless time.

‡Millimeters displacement divided by duration of excitation.

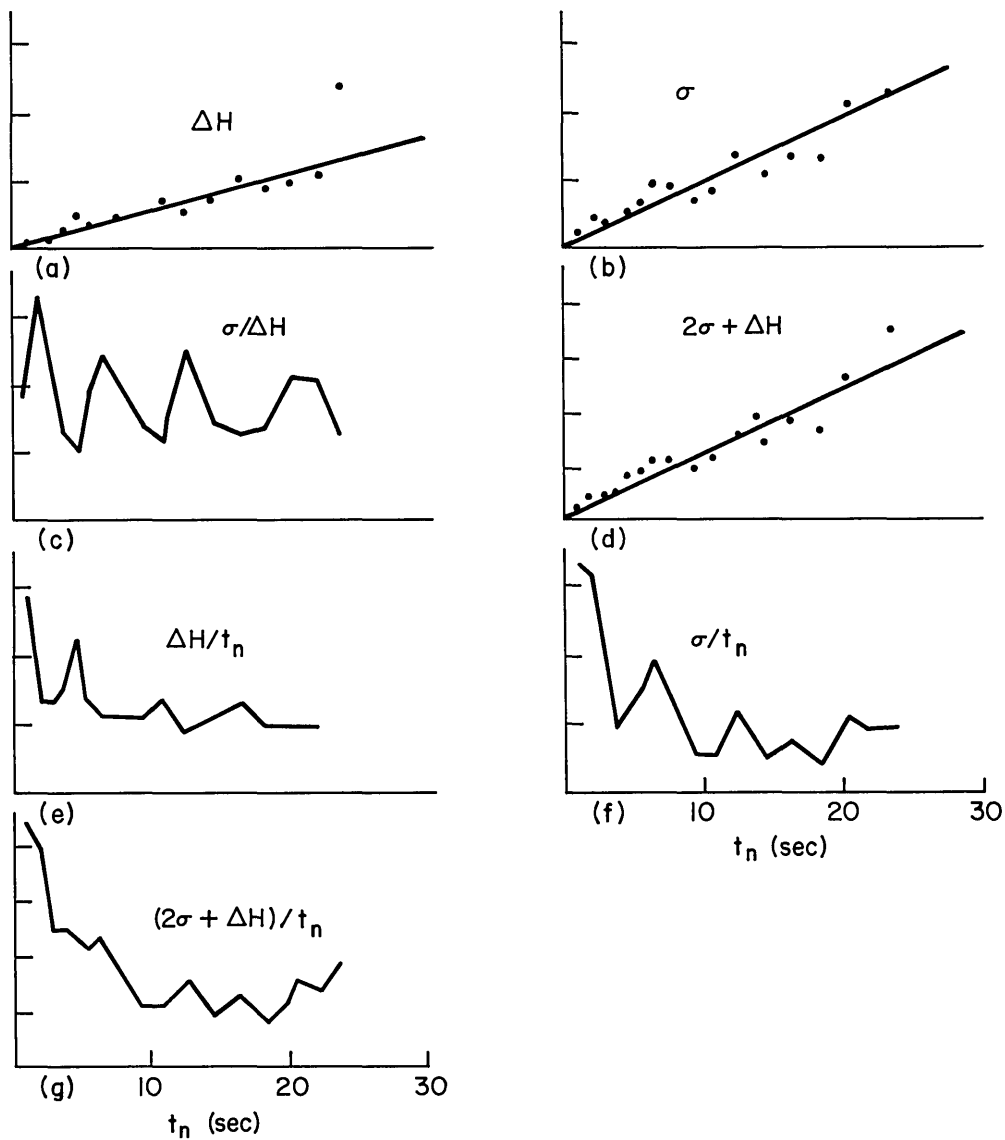


Fig. 11 — Various relationships between average displacement  $\Delta H$ , cyclic components,  $\sigma$ , and excitation time  $t_n$  (same as Fig. 10, but for 4-7 (1-16)). (a)  $\Delta H$  vs  $t_n$ , (b)  $\sigma$  vs  $t_n$ , (c)  $\sigma/\Delta H$  vs  $t_n$ , (d)  $(2\sigma + \Delta H)$  vs  $t_n$ , (e)  $\Delta H/t_n$  vs  $t_n$ , (f)  $\sigma/t_n$  vs  $t_n$ , (g)  $(2\sigma + \Delta H)/t_n$  vs  $t_n$ .

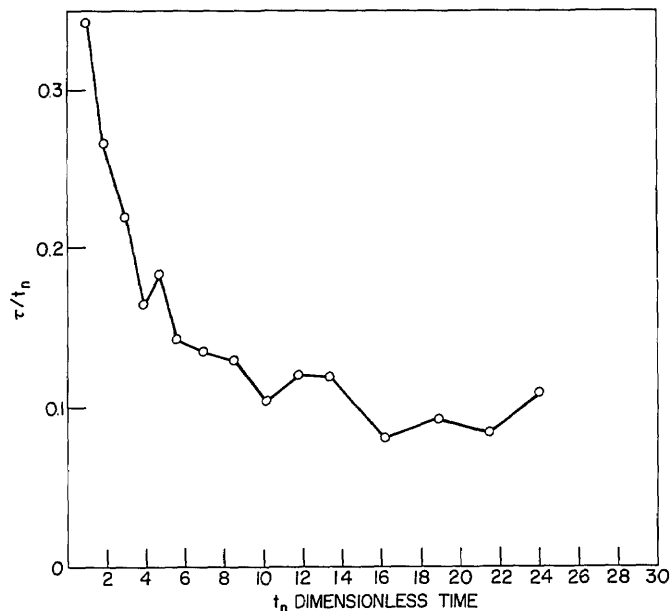


Fig. 12 — Composite plot of  $\sigma/t_n$  vs  $t_n$  showing average of data for runs 3-25 (1-15) and 4-7 (1-16) to illustrate enhanced efficiency of impulsive wave generation at short excitation times. The section of the curve shown is about equal to one Väisälä period, showing that excitation efficiency is greatest where  $t_n/t_V \leq 1/4$ .

drawn through the observed points, and this line passes through the origin.\* This finding supports the view that the process responsible for the depression of the isotherm above the mixed region (measured as  $\Delta H$ ) begins at the starting time of the mixer excitation: it is not compatible with a physical model which requires expansion of a mixed region to a maximum value, prior to the initiation of flow processes which result in depression of isotherms initially outside the stirred region.

The averaged values of points plotted on Fig. 13 were well fitted by

$$\log 100(1 - \Delta H) = 2.00 - kt_n,$$

where the proportionality constant  $k$  has an arithmetic mean of 0.0486. Values of  $k$  for successive time intervals are given in column 5 of Table 6, with percentage deviations in column 6. There is a very slight tendency for  $k$  to droop at short excitation times. However, the droop is considered mechanistically insignificant, since the ratio predicted from a pure wake-collapse mechanism where  $\Delta H = 0$  until after maximum expansion has been attained is close to zero. In column 7, the percentage deviations were recomputed separately for the first 5 and the next 18 points, the last 2 points having been omitted as deviants attributable to normalization errors. On this basis, the slope ratio of the two segments was 1:1.30. The distribution of deviations with time is plotted in Fig. 15. The significance, if any, of the strong periodicity is not understood.

\*Since the scale of the ordinant is logarithmic, the "origin" is taken at  $t = 0$ , and  $\Delta H = 0$  where  $100 - \Delta H = 100$ .

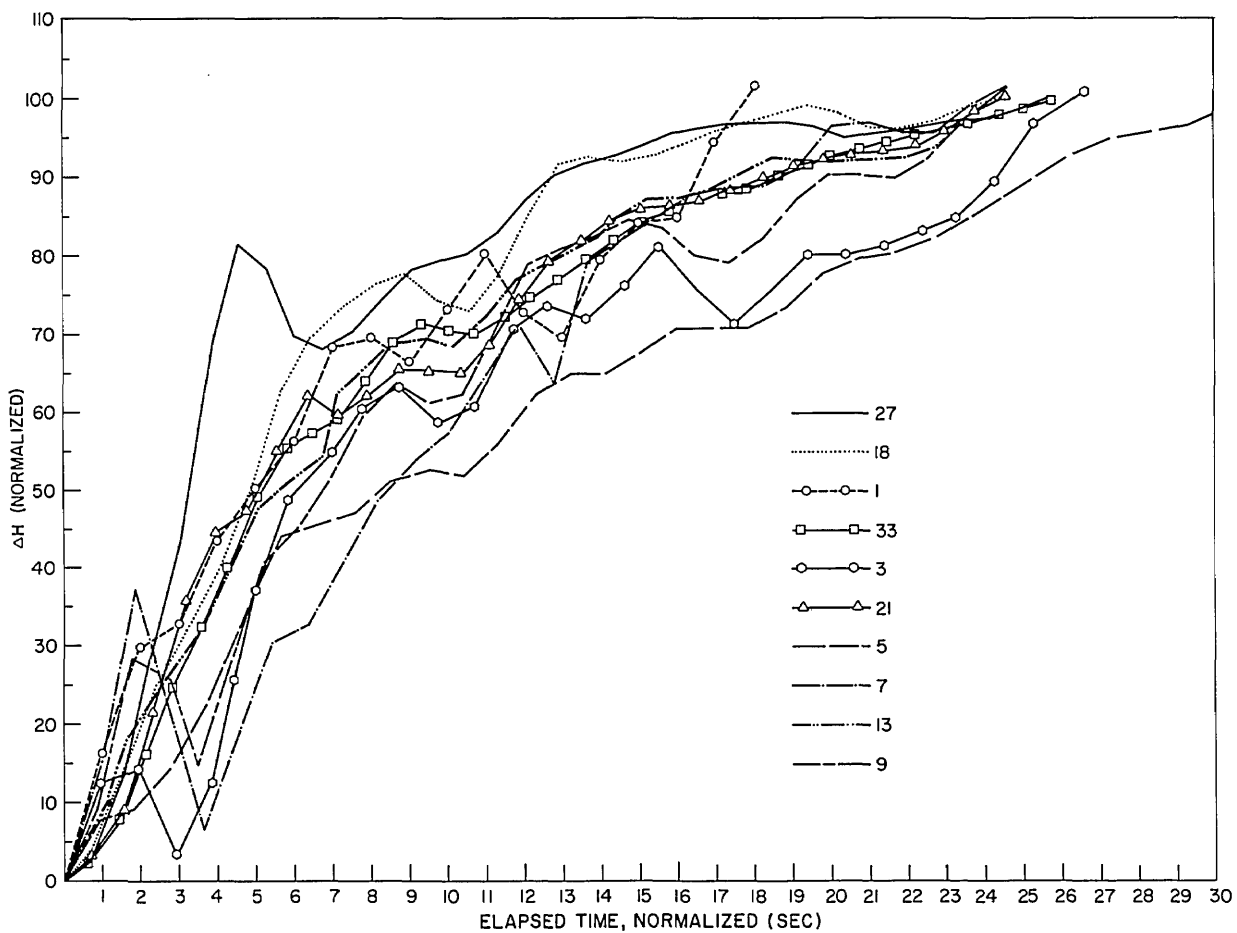


Fig. 13 — Cumulative sum of  $\Delta H$  plotted against normalized excitation time  $t_n$  for 10 runs from series 4-7 (1-16).  $\Delta H$  was normalized to bring upper end of curves to  $\Delta H = 100$ .  $t_e$  is indicated for each curve.

Table 6  
Data Calculations for Figure 14

Excitation Time Group	$\overline{\Delta H}$ ( $\times 10^2$ )	$100 - \overline{\Delta H}$ ( $\times 10^2$ )	$\log (1.00 - \Delta H)100$	$k^*$	Deviation (%)	
					Overall†	Grouped‡
1	6.35	93.6	1.971	0.029	40.3	24.6
2	16.97	83.1	1.920	0.040	17.7	4.00
3	21.89	78.1	1.893	0.035	27.9	9.09
4	31.61	68.4	1.835	0.041	15.6	6.49
5	41.78	58.2	1.765	0.047	3.20	<u>22.08</u>
6	51.22	48.8	1.688	0.052	7.00	3.88
7	55.68	44.3	1.646	0.050	2.88	0.11
8	60.72	39.3	1.594	0.050	2.88	0.11
9	66.33	33.7	1.528	0.052	7.00	3.88
10	66.55	33.5	1.525	0.047	3.20	6.10
11	66.93	33.1	1.520	0.043	11.50	14.09
12	73.00	27.0	1.431	0.047	3.20	6.10
13	78.27	21.7	1.338	0.050	2.88	0.11
14	79.72	21.3	1.308	0.049	0.82	2.10
15	82.37	17.6	1.246	0.050	2.88	0.11
16	85.75	14.2	1.152	0.053	9.05	5.88
17	84.22	15.8	1.199	0.047	3.20	6.10
18	87.50	12.5	1.097	0.050	2.88	0.11
19	89.83	10.1	1.004	0.052	7.00	3.88
20	91.10	8.9	0.949	0.052	7.00	3.88
21	92.68	7.3	0.863	0.054	11.1	7.88
22	93.0	7.0	0.845	0.052	7.00	3.88
23	93.4	6.6	0.819	0.051	4.93	1.89
24	96.0	4.0	0.602	0.058	19.34	—
25	97.6	2.4	0.380	0.064	31.6	—

$$* k = \frac{2.0 - \log 100 (1 - \Delta H)}{t_e} ; \text{ overall av. } 0.0486.$$

$$\dagger \frac{(0.0486 - n)}{0.0486} \times 100.$$

$$\ddagger \frac{(0.0385 - n)}{0.0385} \times 100 \text{ for first 5 values; av. } = 0.0385 \pm 13\%.$$

$$\frac{(0.0512 - n)}{0.0512} \times 100 \text{ for remaining values; av. } = 0.0512 \pm 3.9\%.$$

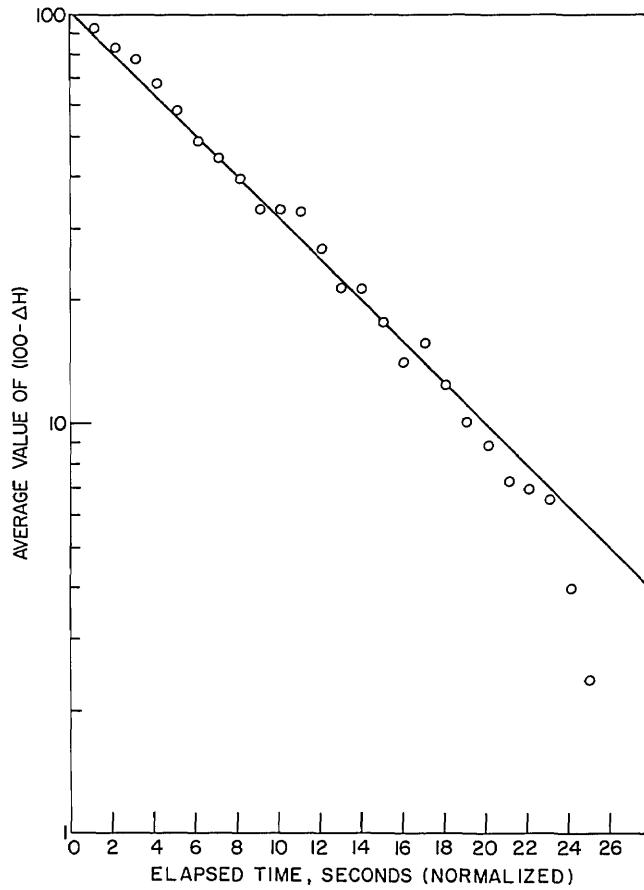


Fig. 14 — Average values of  $\Delta H$  (from Fig. 13) for equal time intervals vs elapsed time

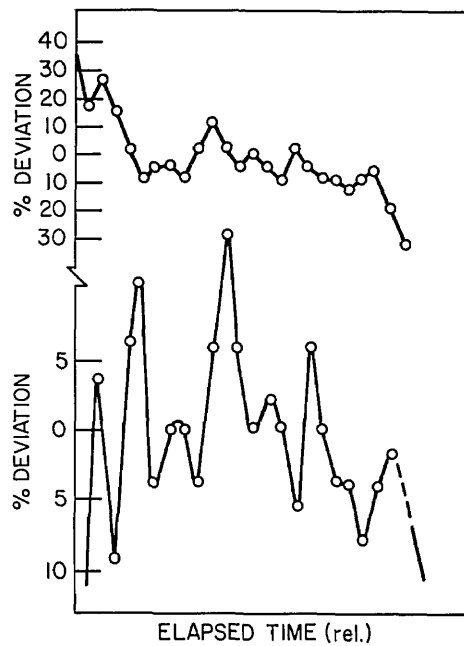


Fig. 15 — Distribution of percentage deviation from straight line of individual points in Fig. 14. Upper curve assumes single, continuous line; lower curve assumes different slopes for the first 5 vs the next 18 points.

## EFFECT OF GENERATOR ROTATIONAL VELOCITY

Four runs were made to estimate the effect of rotational velocity of the generator on the amplitude of the radiated wave field. For these experiments, the thermistor was moved 7.5 mixer diameters away from the axis of the mixer and placed nearer the centerline depth to avoid large changes of  $\Delta H$ . The results are given in Table 7. From the constancy of the ratio in the last column, it appears that the system response, and presumably the source strength, is proportional to the angular velocity of the mixer, and hence, to the average surface velocity. Since the excitation time was constant for this series (3 s), the source has the dimensions of length (rad/s  $\times$  radius  $\times$  time). This suggested a review of the data presented earlier (page 7) for the mesh cylinder generator. The ratio of the "average displacement" to the distance of travel of the periphery of the mixer  $D_m$  was computed; results are in Table 8. The roughly constant ratio, with one major exception, tends to support the immediately preceding result. The average deviation is higher since the data were from a less homogeneous grouping of source conditions, including excitation times from 2.5 to 7.5 s, angular velocities of 10.2 to 27.9 rad/s, and from 1 to 5 cycles of the generator. From these results it appears that the basic source strength can be expressed in terms of rather simple relationships, in this case excitation time and surface velocity.

## WAVE PROPAGATION

A point of special interest in the group of runs under discussion was the question of whether or not the wave field, at points remote from the generator, exhibited characteristics compatible with immediate excitation. To test this, several groups of runs were made with the measurement point at various depths and lateral displacements from the generator. It was found that  $\Delta H$  became small outside the local wake collapse region and that the apparent harmonic content of the propagating waves diminished with increasing travel distances. The relationship between apparent wave velocity and distance from the source was examined by measuring the arrival time of the first major inflection point at several distances from the generator and at a depth of 5 cm. The results are given in Table 9 and in Fig. 16.

The apparent mean velocity  $V$  represents the distance of travel to the measurement point divided by the travel time.\* Since the waves are dispersive, this mean velocity varies with distance of travel. The relationship  $V \approx k\sqrt{x}$  was found to hold where  $x$  is the lateral displacement of the measurement point from the generator and  $k$  is the proportionality constant, values of which are given in the tabulation (following page). Since  $V = k\sqrt{x}$ , the arrival time  $t = x/V = x/k$ , implying initiation at  $t = 0$ , confirming immediate excitation of a radiating wave field. It is suspected that  $k$  will vary with the absolute density gradient and curvature of the gradient, but no systematic investigation of this was made. During this series, it was noted also that the wave amplitude near the surface seemed to be quite contingent on the curvature of the near-surface gradient; where the gradient became increasingly stable toward the surface, the amplitude of waves measured at shallow depths (e.g., 5-20 mm) tended to be larger than in cases where the gradient became decreasingly stable toward the surface. This observation was not examined further.

---

\*Some ambiguity may be expected as a result of possible confusion between group and phase velocities; when the leading apparent wave has separated into an advancing group, the speed of advance contains cyclic variations, reflecting the changing phase of the leading disturbance.

Table 7  
Internal Wave Properties for Various Mixer Speeds

Run No.	Speed Setting	Mixer Speed (rad/s)	$\Delta H$ (mm)	$\sigma$ (mm)	$(2\sigma + \Delta H)$ (mm)	$(2\sigma + \Delta H)$ (rad/s)
1	Max	5.08	0.417	3.124	6.66	1.31
2	90	3.42	0.540	2.08	4.70	1.37
3	75	2.74	0.094	2.12	4.32	1.58
4	60	1.91	0.025	1.087	2.424	1.27

Table 8  
Internal Wave Amplitude, Paddle Mixer

Run No.	$D_m$ (cm)	Av. Isotherm Displacement (mm)	Av. Displacement/ $D_m$ (mm)
3-18-1	76	6.95	0.091
2	76	6.67	0.088
3	76	7.34	0.096
4	25	3.73	0.149
5	25	9.01	(0.372)
6	126	8.88	0.070

Table 9  
Apparent Velocity of Internal Waves

Run No.	Distance from Generator (mm)	Arrival Time (s)	Apparent Velocity (cm/s)	$k$
4-2-1(5)	12	10	1.2	0.346
4-2-2(5)	75	24	3.13	0.361
4-2-3(5)	150	35	4.29	0.350
4-2-4(5)	300	52	5.77	0.333
Average	—	—	—	0.348

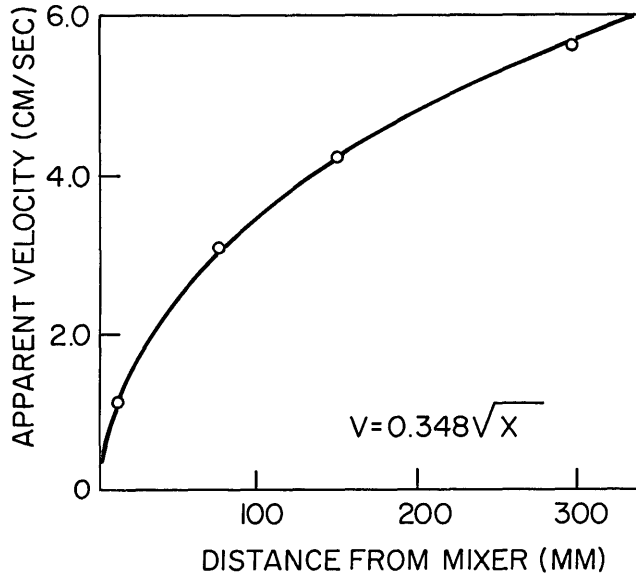


Fig. 16 — Velocity of radiated “apparent” internal waves vs distance from generator. Curve indicates parabolic waveform for advancing front.

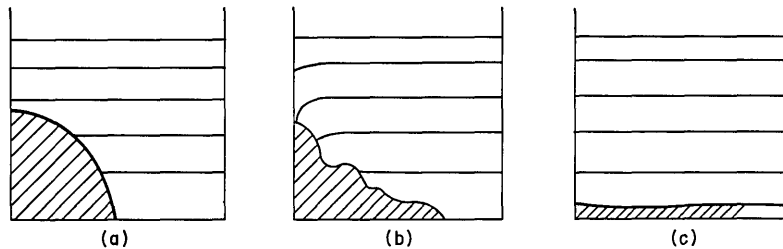


Fig. 17 — Sketch of isopycnal displacements in response to noncyclic components of collapse flow

## DISCUSSION

### Background and Definitions

The formal theoretical concept set forth in the original publication of Schooley and Stewart (5) was later studied in controlled laboratory conditions by Wu (3), who used two sources: a mixer similar to the one employed for the present experiments, and a gated semicylindric region of constrained mixed water. However, most of his published results describe only the response of the stratified fluid system to the instantaneous release of water from the gated source. This experiment is a nearly exact physical realization of the mathematical model used by Wessel (2). In these two models, the only primary driving force available for collapse and spread of the mixed fluid and the production of internal waves is the action of gravity on the buoyancy imbalance between the mixed fluid region and the external ambient fluid. It follows that no collapse, no isotherm displacement and no generation of internal waves can occur before the constraints which support the density imbalance are released. It also follows that the first tiny movement of fluid, once the constraint is released, initiates a wavelike process which extends its influence throughout the experimental basin at a rate governed by the fluid properties. This has consequences which will be discussed in relation to the schematic of Fig. 17, representing one quarter of an idealized mixed region in its initial, partially collapsed, and fully collapsed states.

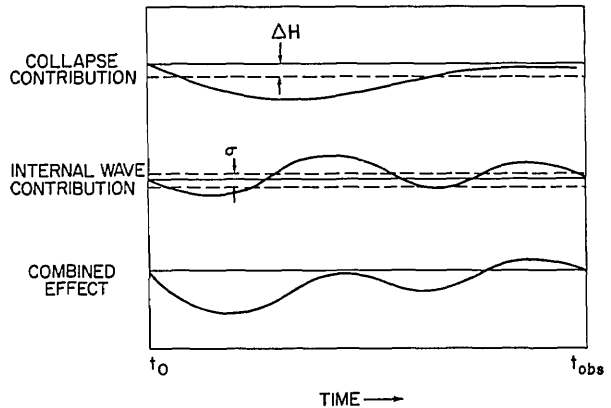


Fig. 18 — Sketch of time histories in wake collapse record, defining observed distinction between noncyclic and internal wave effects

The assumed symmetry in Fig. 17 implies horizontal and vertical separation planes passing through the origin, with free slip. In this situation, maintaining continuity requires a noncyclic component of flow vertically downward along the  $y$  axis and horizontally outward along the  $x$  axis in response to collapse of the mixed region. Thus a density sensor slightly above the mixed region on the  $y$  axis would necessarily register an initial downward shift in the local isopycnal. This downward flow would persist as long as the noncyclic component of collapse continued, and it would have a time-dependent displacement  $\Delta H$  which would be related to the time integral of downward velocity at the point of measurement. At some point in time, assuming a basin of finite dimensions,  $\Delta H$  would necessarily pass through a maximum value and gradually return toward its final equilibrium level. In addition to the directed flow component, a variety of cyclic wavelike processes could be superimposed and the time history of the density record could contain information relating to the basic collapse process and to any waves generated by the collapse process. We distinguish the directed flow components as *collapse flow*, used herein to refer only to any non-oscillatory flow component of the collapse process, and *internal waves*, a term which refers to all cyclic processes. Successive instantaneous values of isopycnal displacement at the measurement point, averaged over a finite but short observation interval  $t_{obs}$  is  $\Delta H$ ; the root mean square average of the cyclic displacement is designated  $\sigma$ . Consider now the nature of the two time histories: at  $t = 0$ , both  $\Delta H$  and  $\sigma$  are zero, and both start to increase as the initial constraints on the mixed region are released. The gross features of the subsequent histories of these two quantities are similar in that both increase from zero to a maximum value and then decrease, asymptotically approaching zero. However, the detailed time histories at the measurement point are composite because the instantaneous displacement is the sum of contributions from both collapse flow and internal waves. The mean values of the collapse and oscillating terms, averaged over the observation period  $t_{obs}$ , are determinate. An illustrative case is sketched in Fig. 18.

Starting with only the time history, information about the separate contributions of collapse flow and waves can be obtained by using standard statistical methods. The mean displacement of the record from its initial level is determined by averaging numerous measurements of displacement made at equal intervals throughout the observation period over the interval  $t_{obs}$ . Where  $t_{obs}$  is long compared to the collapse time, the mean value of  $\Delta H$  is proportional to the integrated area under the measured curve. Assuming thermocline displacement to be approximately linear with downward flow, the area  $\Delta H \times t_{obs}$  is proportional to the source strength, the total collapse flow (and hence proportional to the buoyancy gradient), and other parameters which determine the volume of mixed water and the efficiency of mixing. The standard deviation from the mean of a set of sequential

individual measurements then represents the magnitude of the cyclic components, or internal waves. Thus,  $\Delta H$  and  $\sigma$  permit characterization of the magnitude of two processes which are of special interest to the analysis of the collapsing wake. A third measurement of significance can be derived from the cumulative sum of deviations from the zero level in the time histories of isopycnal displacement. Individual deviations for successive measurements made at equal intervals of time over the observation period are simply added algebraically in sequence, and the running total is plotted against the number of measurements included in the sum. This gives a curve which starts from zero at  $t = 0$ , rises from the baseline, and eventually approaches some limiting value. Much variability is possible in the details of the curve, particularly where  $\sigma$  is large compared to  $\Delta H$ , but the net effect of averaging over a range of values of  $t_e/t_{obs}$  is to reduce the apparent contribution from the internal waves. The point at which  $\Delta H$  has attained its maximum value and has started to decrease represents a characteristic time of the collapse process.

### Interpretation of Experimental Results

The results presented, plus visual observations, point toward a coherent physical model of growth and collapse which differs in significant detail from the classical theoretical model. Agitation of the mixer, with dye tracers in the water, leads to a visually obvious mixed region, initially of nearly circular cross section. This mixed region expands visibly faster in the horizontal than in the vertical dimension, and then collapses vertically while continuing to spread horizontally for a finite time. The cross section of the collapsed wake varies from run to run, but usually appears as a flattened ellipse or diamond.\* There was no reasonable doubt that the dyed water exhibited a behavior fully compatible, in a qualitative sense, with the collapsing wake model: in addition to expansion and collapse of a mixed region, internal waves were observed which had appropriate amplitudes, periods, and propagation characteristics.

Despite this "visual similarity," no vertical temperature profiles could be measured which were fully compatible with the concept of a quiescent well-mixed region. Those profiles which were made two or three Väisälä periods after agitation of the mixer showed only wavelike disturbances with no clearly recognizable zone of anomalous density. Profiles made over time intervals smaller than the Väisälä period showed pronounced and erratic displacements of the isotherms, often with high-frequency components attributed to turbulence. When these temperature variations were observed at a single point within the wake, it became apparent that small-scale mixing, while visually evident, was much less obvious in temperature records of growth and collapse of the mixed region than were motions of larger scale. This is illustrated by the time histories of wake development (e.g., Fig. 4). The rapidly fluctuating movements associated with intense and relatively small-scale turbulent motions are superimposed on motions of a grander scale which progressively lose the randomness of turbulence and gently ease into the more stately rhythms of internal waves. The region in which the temperature plots have pulled together, 4 to 8 s after initiation of the mixing, represents the region of greatest vertical expansion of the wake; colder water has been projected upward to the shallower and initially warmer measurement points, and warm water has been projected downward to the deepest measuring point. The maximum growth of the wake appears at between 5 and 7.5 s after agitation,

---

\*Complex horizontal shear layers, much like those reported by Woods (6), also occur in the tank. These often result in asymmetric dye displacements if their velocities are significantly large.

but the precise point of maximum vertical extension seems to be inherently indeterminate; the relative phase of large-scale motions (dimensions like the local radius) varies with time and with the location of the measurement point. The maximum growth point, therefore, has only a statistical meaning and does not characterize an instantaneous condition of real wakes. The observed maxima, however, are roughly compatible with van de Watering's estimate (4) of  $0.2 t_V$ ; the estimated Väisälä period is 27.5 s and the observed maxima lie between 0.19 and  $0.27 t_V$ .

The same sort of considerations apply to the concept of mixing within the wake; any time series of measurements taken within the wake cross section can be extended or repeated to produce an approximately constant value of mean displacement for a specified time interval, and such measurements can be integrated across the cross section to produce a numeric estimate of the "degree of mixing."

While such an estimate does have demonstrable statistical significance, it seems to have little physical significance; the instantaneous distribution was not found to be in accord with the gross statistical picture. Water moves inward in relatively discrete masses from the boundaries of the wake to compensate for that which moves outward from inside the wake. The dimensional scale of these processes extends through a cascade of scales with dimensions up to a maximum corresponding to the local wake diameter, and a more usually observed maximum about equal to the local radius. The small-scale processes determine the distribution of dye, the larger scales determine the dynamic condition of the wake. Outside the region of turbulent mixing, defined as the zone in which dye tracers are distributed by small-scale turbulence, it is observed that predominant temperature disturbances, or thermocline displacements, are essentially free of small-scale, high-frequency components, and exhibit only gentle wavelike undulations which are often in phase with turbulent bursts or puffs. However, two separate cases must be distinguished: (a) At lateral positions well separated from the turbulent region, the waves behave classically. (These were observed in preliminary experiments where an expanding and collapsing rubber tube was used as a perturbation source.) It is believed that these waves represent, in the first instance, the initial response of the resonant fluid mass to movement of the mixer. (b) In areas close to the axis of the mixed region, but above the turbulent region, the initial response is indicative of a downward flow which depresses the isotherm in which the sensor is initially placed. This displacement occurs almost immediately on excitation of the turbulence generator, and is well established *before* the vertical growth of the wake has reached a maximum, and certainly before collapse, in the usual sense, has begun.

The above relationships were not very clear in experiments made with the original hardware-cloth mixer because of the wide range of energetic scales near the source. The mixer paddles introduced a "noise level" into the near field which was too high to deal with successfully. Fortunately a great improvement occurred on adoption of the spiral-wire source (e.g. compare Fig. 4 with Fig. 7). With this mixer, even the earliest stages of expansion followed a smooth and rhythmic development which blended harmoniously into the total wave field. One important feature of the spiral-wire mixer is that the configuration makes it difficult to "flip-off" directed vortexes of preferred angular orientation. This means that the outward progression of turbulence occurs on a dimensional scale which is more or less independent of the mixer characteristics once the first half-cycle of its rotation has been accomplished. For this reason it must be assumed that the characteristic expansion pattern is inherently determined by some characteristic of the system other than the mixer, except for very short excitation times where the mixer rotation does not

complete a full cycle. We take the results, therefore, to indicate that an initial bias becomes operative immediately on excitation, establishing a pattern of semidirected flow which is then augmented by the continuing processes of wake expansion and collapse. At the present time, we speculate that this bias arises from the asymmetry introduced into the situation by the density gradient: Flows directed radially outward from the generator are unrestricted in the horizontal, but work against gravity via the buoyancy changes, in the vertical. Also, inertial components of flow vary slightly with the local water density. The net result involves a progressive shift of momentum from vertical to horizontal flow components, tightly phased into the wave motions generated by the impulsive movement of the generator as it was first activated.

## CONCLUSION

Any rigorous theory which can account for the phenomenon observed must deal with the following:

1. An instantaneous impulsive generation of internal waves which propagate through the external fluid.
2. Immediate onset of flow downward over the wake axis and outside the region of primary mixing, accompanied by horizontal flow outward at the axial depth.
3. A variable partition of energy between that contained in the radiating internal wave field and that stored as potential energy in the mixed region, the partition coefficient being dependent on the ratio of excitation time to local Väisälä period.

## RECOMMENDATION

Extension of this work, coupled with mathematical analysis to develop a suitable wake model, is recommended.

## REFERENCES

1. F.H. Harlow, "The Particle-in-Cell Computing Method for Fluid Dynamics," in *Methods in Computational Physics* Vol. III, Academic Press, New York, 1964, p. 319; see also "Fluid Dynamics," Los Alamos Scientific Laboratories Monograph LA 4700 UC-34, June 1971.
2. W.R. Wessel, "Numerical Study of the Collapse of a Perturbation in an Infinite Density-Stratified Fluid," in *High Speed Computing in Fluid Dynamics: The Physics of Fluids, Suppl. II*, 171-76 (1969).
3. J. Wu, "Flow Phenomena Caused by the Collapse of a Mixed Region in a Density-Stratified Medium," Technical Report 231-11, Hydronautics Inc., Laurel, Md., Mar. 1966.
4. W.P.M. van de Watering, M.P. Tulin, and J. Wu, "Experiments on Turbulent Wakes in a Stable Density-Stratified Environment," Technical Report 231-24, Hydronautics, Inc., Feb. 1969.

5. A.H. Schooley and R.W. Stewart, "Experiments with a Self-Propelled Body Submerged in a Fluid with a Vertical Density Gradient," *J. Fluid Mech.* 15, 83-96 (1963).
6. J.D. Woods, "Wave-Induced Shear Instability in the Summer Thermocline," *J. Fluid Mech.* 32 (Part 4), 791-800 (1968).

## DOCUMENT CONTROL DATA - R &amp; D

(Security classification of title, body of abstract and indexing annotation must be entered when the overall report is classified)

1. ORIGINATING ACTIVITY (Corporate author) Naval Research Laboratory Washington, D.C. 20375		2a. REPORT SECURITY CLASSIFICATION Unclassified	
		2b. GROUP	
3. REPORT TITLE ON THE GROWTH AND COLLAPSE OF MIXED REGIONS IN STRATIFIED FLUIDS			
4. DESCRIPTIVE NOTES (Type of report and inclusive dates) A final report on one phase of a continuing problem.			
5. AUTHOR(S) (First name, middle initial, last name) K. G. Williams			
6. REPORT DATE September 25, 1973		7a. TOTAL NO. OF PAGES 38	7b. NO. OF REFS 6
8a. CONTRACT OR GRANT NO. NRL G01-06		9a. ORIGINATOR'S REPORT NUMBER(S) NRL Report 7586	
b. PROJECT NO. W-11-125-703		9b. OTHER REPORT NO(S) (Any other numbers that may be assigned this report)	
c.			
d.			
10. DISTRIBUTION STATEMENT Approved for public release; distribution unlimited.			
11. SUPPLEMENTARY NOTES		12. SPONSORING MILITARY ACTIVITY Department of the Navy (Naval Air Systems Command) Washington, D.C. 20361	
13. ABSTRACT Experimental observations were made of the development of a mechanically generated, mixed region in the interior of a density-stratified fluid. The results showed that internal waves were initiated in the exterior unmixed fluid before the mixed region reached its maximum vertical extent and began to collapse.			

14. KEY WORDS	LINK A		LINK B		LINK C	
	ROLE	WT	ROLE	WT	ROLE	WT
Wake collapse Internal waves Turbulent wake Mixed region collapse						